

# Optoelectronic Reservoir Computing

Y. Paquot<sup>1\*</sup>, F. Duport<sup>1\*</sup>, A. Smerieri<sup>1\*</sup>, J. Dambre<sup>2</sup>,  
B. Schrauwen<sup>2</sup>, M. Haelterman<sup>1</sup>, S. Massar<sup>3†</sup>

<sup>1</sup>*Service OPERA-photonique, Université libre de Bruxelles (U.L.B.),  
50 Avenue F. D. Roosevelt, CP 194/5, B-1050 Bruxelles, Belgium*

<sup>2</sup>*Department of Electronics and Information Systems (ELIS),  
Ghent University, Sint-Pietersnieuwstraat 41, 9000 Ghent, Belgium.*

<sup>3</sup>*Laboratoire d'Information Quantique (LIQ),  
Université libre de Bruxelles (U.L.B.),  
50 Avenue F. D. Roosevelt, CP 225, B-1050 Bruxelles, Belgium*

*\*These authors contributed equally to this work and*

*† Corresponding author: smassar@ulb.ac.be*

## Abstract

Reservoir computing is a recently introduced, highly efficient bio-inspired approach for processing time dependent data. The basic scheme of reservoir computing consists of a non linear recurrent dynamical system coupled to a single input layer and a single output layer. Within these constraints many implementations are possible. Here we report an opto-electronic implementation of reservoir computing based on a recently proposed architecture consisting of a single non linear node and a delay line. Our implementation is sufficiently fast for real time information processing. We illustrate its performance on tasks of practical importance such as nonlinear channel equalization and speech recognition, and obtain results comparable to state of the art digital implementations.

## I. INTRODUCTION

The remarkable speed and multiplexing capability of optics makes it very attractive for information processing. These features have enabled the telecommunications revolution of the past decades. However, so far they have not been exploited insomuch as computation is concerned. The reason is that optical nonlinearities are very difficult to harness: it remains challenging to just demonstrate optical logic gates, let alone compete with digital electronics[1]. This suggests that a much more flexible approach is called for, which would exploit as much as possible the strenghts of optics without trying to mimic digital electronics. Reservoir computing [2–10], a recently introduced, bio-inspired approach to artificial intelligence, may provide such an opportunity.

Here we report the first experimental reservoir computer based on an opto-electronic architecture. As nonlinear element we exploit the sine nonlinearity of an integrated Mach-Zehnder intensity modulator (a well known, off-the-shelf component in the telecommunications industry), and to store the internal states of the reservoir computer we use a fiber optics spool. We report results comparable to state of the art digital implementations for two tasks of practical importance: nonlinear channel equalization and speech recognition.

Reservoir computing, which is at the heart of the present work, is a highly successful method for processing time dependent information. It provides state of the art performance for tasks such as time series prediction [4] (and notably won a financial time series prediction competition[11]), nonlinear channel equalization [4], or speech recognition [12–14]. For some of these tasks reservoir computing is in fact the most powerful approach known at present.

The central part of a reservoir computer is a nonlinear recurrent dynamical system that is driven by one or multiple input signals. The key insight behind reservoir computing is that the reservoir’s response to the input signal, i.e., the way the internal variables depend on present and past inputs, is a form of computation. Experience shows that in many cases the computation carried out by reservoirs, even randomly chosen ones, can be extremely powerful. The reservoir should have a large number of internal (state) variables. The exact structure of the reservoir is not essential: for instance, in some works the reservoir closely mimics the interconnections and dynamics of biological neurons in a brain [6], but many other architectures are possible.

To achieve useful computation on time dependent input signals, a good reservoir should

be able to compute a large number of different functions of its inputs. That is, the reservoir should be sufficiently high-dimensional, and its responses should not only depend on present inputs but also on inputs up to some finite time in the past. To achieve this, the reservoir must operate at the threshold of dynamical instability which ensures that the system exhibits a “fading memory”, meaning that it will gradually forget previous inputs.

Reservoir computing is a versatile and flexible concept. This follows from two key points: 1) many of the details of the nonlinear reservoir itself are unimportant except for the dynamic regime (threshold of instability) which can be tuned by some global parameters; and 2) the only part of the system that is trained is a linear output layer. Because of this flexibility, reservoir computing is amenable to a large number of experimental implementations. Thus proof of principle demonstrations have been realized in a bucket of water [15] and using an analog VLSI chip [16], and arrays of semiconductor amplifiers have been considered in simulation [17]. However, it is only very recently that an analog implementation with performance comparable to digital implementations has been reported: namely, the electronic implementation presented in [18].

Our experiment is based on a similar architecture as that of [18], namely a single non linear node and a delay line. The main differences are the type of non linearity and the desynchronisation of the input with respect to the period of the delay line. These differences highlight the flexibility of the concept. The performance of our experiment on two benchmark tasks, isolated digit recognition and non linear channel equalization, is comparable to state of the art digital implementations of reservoir computing. Compared to [18], our experiment is almost 6 orders of magnitude faster, and a further 2-3 orders of magnitude speed increase should be possible with only small changes to the system.

The flexibility of reservoir computing and its success on hard classification tasks makes it a promising route for realizing computation in physical systems other than digital electronics. In particular it may provide innovative solutions for ultra fast or ultra low power computation. In Supplementary Material 1 we describe reservoir computing in more detail and provide a road map for building high performance analog reservoir computers. In the discussion we discuss how to measure the speed of experimental reservoir computers.

## II. RESULTS

### A. Principles of Reservoir Computing

Before introducing our implementation, we recall a few key features of reservoir computing; for a more detailed treatment of the underlying theory, we refer the reader to Supplementary Material 1.

As is traditional in the literature, we will consider tasks that are defined in discrete time, e.g., using sampled signals. We denote by  $u(n)$  the input signal, where  $n \in \mathbb{Z}$  is the discretized time; by  $\bar{x}(n)$  the internal states of the system used as reservoir; and by  $\hat{y}(n)$  the output of the reservoir. A typical evolution law for  $\bar{x}(n)$  is  $\bar{x}(n+1) = f(\mathbf{A}\bar{x}(n) + \bar{m}u(n))$ , where  $f$  is a nonlinear function,  $\mathbf{A}$  is the time independent connection matrix and  $\bar{m}$  is the time independent input mask. Note that in our work we will use a slightly different form for the evolution law, as explained below.

In order to perform the computation one needs a readout mechanism. To this end we define a subset  $x_i(n)$ ,  $0 \leq i \leq N-1$  (also in discrete time) of the internal states of the reservoir. It is these states which are observed and used to build the output. The time dependent output is obtained in an output layer by taking a linear combination of the internal states of the reservoir  $\hat{y}(n) = \sum_{i=0}^{N-1} W_i x_i(n)$ . The readout weights  $W_i$  are chosen to minimize the Mean Square Error (MSE) between the estimator  $\hat{y}(n)$  and a target function  $y(n)$ :

$$MSE = \frac{1}{L} \sum_{n=1}^L (y(n) - \hat{y}(n))^2 \quad (1)$$

over a set of examples (the training set). Because the MSE is a quadratic function of the  $W_i$  the optimal weights can be easily computed from the knowledge of  $x_i(n)$  and  $y(n)$ . In a typical run, the quality of the reservoir is then evaluated on a second set of examples (the test set). After training, the  $W_i$  are kept fixed.

### B. Principles of our implementation

In the present work we use an architecture related to that used in [18] and to the minimum complexity networks studied in [19]. As in [18], the reservoir is based on a non-linear system with delayed feedback (a class of systems widely studied in the nonlinear dynamics

community, see e.g. [20]) and consists of a single nonlinear node and a delay loop. The information about the previous internal state of the reservoir up to some time  $T$  in the past is stored in the delay loop. After a period  $T$  of the loop, the entire internal state has been updated (processed) by the nonlinear node. In contrast to the work described in [18], the nonlinear node in our implementation is essentially instantaneous. Hence, in the absence of input, the dynamics of our system can be approximated by the simple recursion

$$x(t) = \sin(\alpha \cdot x(t - T) + \varphi) \quad (2)$$

where  $\alpha$  (the *feedback gain*) and  $\varphi$  (the *bias*) are adjustable parameters and we have explicitly written the sine nonlinearity used in our implementation.

We will use this system to perform useful computation on input signals  $u(n)$  evolving in discrete time  $n \in \mathbb{Z}$ . As the system itself operates in continuous time, we need to define ways to convert input signal(s) to continuous time and to convert the system's state back to discrete time. The first is achieved by using a sample and hold procedure. We obtain a piecewise constant function  $u(t)$  of the continuous variable  $t$ :  $u(t) = u(n)$ ,  $nT' \leq t < (n + 1)T'$ . The time  $T' \leq T$  is taken to be less than or equal to the period  $T$  of the delay loop; when  $T' \neq T$  we are in the unsynchronised regime (see below). To discretize the system's state, we note that the delay line acts as a memory, storing the delayed states of the nonlinearity. From this large-dimensional state space, we take  $N$  samples by dividing the input period  $T'$  into  $N$  segments, each of duration  $\theta$  and sampling the state of the delay line at a single point with periodicity  $\theta$ . This provides us with  $N$  *snapshots* of the nonlinearity's response to each input sample  $u(n)$ . From these snapshots, we construct  $N$  discrete-time sequences  $x_i(n) = x(nT' + (i + 1/2)\theta)$  ( $i = 0, 1, \dots, N - 1$ ) to be used as reservoir states from which the required (discrete-time) output is to be constructed.

Without further measures, all such recorded reservoir states would be identical, so for computational purposes our system is one-dimensional. In order to use this system as a reservoir computer, we need to drive it in such a way that the  $x_i(n)$  represent a rich variety of functions of the input history. It is often helpful [9, 19] to use an “input mask” that breaks the symmetry of the system. In [18] good performance was improved by using a nonlinear node with an intrinsic time scale longer than the time scale of the input mask. In the present work we also use the “input mask”, but as our nonlinearity is instantaneous, we cannot exploit its intrinsic time scale. We instead chose to desynchronize the input and the

reservoir, that is, we hold the input for a time  $T'$  which differs slightly from the period  $T$  of the delay loop. This allows us to use each reservoir state at time  $n$  for the generation of a new different state at time  $n + 1$  (unlike the solution used in [18] where the intrinsic time scale of the nonlinear node makes the successive states highly correlated). We now explain these important notions in more detail.

The input mask  $m(t) = m(t + T')$  is a periodic function of period  $T'$ . It is piecewise constant over intervals of length  $\theta$ , i.e.,  $m(t) = m_j$  when  $nT' + j\theta \leq t < nT' + (j + 1)\theta$ , for  $j = 0, 1, \dots, N - 1$ . The values  $m_j$  of the mask are randomly chosen from some probability distribution. The reservoir is driven by the product  $v(t) = \beta m(t)u(t)$  of the input and the mask, with  $\beta$  an adjustable parameter (the *input gain*). The dynamics of the driven system can thus be approximated by

$$x(t) = \sin(\alpha x(t - T) + \beta m(t)u(t) + \varphi) \quad (3)$$

It follows that the reservoir states can be approximated by

$$x_i(n) = \sin(\alpha x_i(n - 1) + \beta m_i u(n) + \varphi) \quad (4)$$

when  $T' = T$  (the synchronized regime) or more generally as

$$x_i(n) = \begin{cases} \sin(\alpha x_{i-k}(n - 1) + \beta m_i u(n) + \varphi) & k \leq i < N \\ \sin(\alpha x_{N+i-k}(n - 2) + \beta m_i u(n) + \varphi) & 0 \leq i < k \end{cases} \quad (5)$$

when  $T' = \frac{N}{N+k}T$ , ( $k \in \{1, \dots, N - 1\}$ ) (the unsynchronized regime). In the synchronized regime, the reservoir states correspond to the responses of  $N$  uncoupled discrete-time dynamical systems which are similar, but slightly different through the randomly chosen  $m_j$ . In the unsynchronized regime, with a desynchronization  $T - T' = k\theta$ , the state equations become coupled, yielding a much richer dynamics. With an instantaneous nonlinearity, desynchronisation is necessary to obtain a set of state transformations that is useful for reservoir computing. We believe that it will also be useful when the non linearity has an intrinsic time scale, as it provides a very simple way to enrich the dynamics.

In summary, by using an input mask, combined with desynchronization of the input and the feedback delay, we have turned a system with a one-dimensional information representation into an  $N$ -dimensional system.

### C. Hardware setup

The above architecture is implemented in the experiment depicted in Fig. 1. The sine nonlinearity is implemented by a voltage driven intensity modulator (Lithium Niobate Mach Zehnder interferometer), placed at the output of a continuous light source, and the delay loop is a fiber spool. A photodiode converts the light intensity  $I(t)$  at the output of the fiber spool into a voltage; this is mixed with an input voltage generated by a function generator and proportional to  $m(t)u(t)$ , amplified, and then used to drive the intensity modulator. The feedback gain  $\alpha$  is set by adjusting the average intensity  $I_0$  of the light inside the fiber loop with an optical attenuator. By changing  $\alpha$  we can bring the system to the edge of dynamical instability. The nonlinear dynamics of this system have already been extensively studied, see [21–23]. The dynamical variable  $x(t)$  is obtained by rescaling the light intensity to lie in the interval  $[-1, +1]$  through  $x(t) = 2I(t)/I_0 - 1$ . Then, neglecting the effect of the bandpass filter induced by the electronic amplifiers, the dynamics of the system is given by eq. (3) where  $\alpha$  is proportional to  $I_0$ . Equation (3), as well as the discretized versions thereof, eqs. (4) and (5), are derived in the supplementary material; the various stages of processing of the reservoir nodes and inputs are shown in Fig. 2.

In our experiment the round trip time is  $T = 8.504\mu\text{s}$  and we typically use  $N = 50$  internal nodes. The parameters  $\alpha$  and  $\beta$  in eq. (3) are adjusted for optimal performance (their optimal value may depend on the task), while  $\varphi$  is usually set to 0. The intensity  $I(t)$  is recorded by a digitizer, and the estimator  $\hat{y}(n)$  is reconstructed offline on a computer.

We illustrate the operations of our reservoir computer in Fig.3 where we consider a very simple signal recognition task. Here, the input to the system is taken to be a random concatenation of sine and square waves; the target function  $y(n)$  is 0 for a sine wave and 1 for a square wave. The top panel of Fig. 3 shows the input to the reservoir: the blue line is the representation of the input in continuous time  $u(t)$ . In the bottom panel, the output of the network after training is shown with red crosses, against the desired output represented by a blue line. The performance on this task is essentially perfect: the Normalized Mean Square Error  $NMSE = \frac{1}{L} \sum_{n=1}^L (y(n) - \hat{y}(n))^2 / \frac{1}{L} \sum_{n=1}^L (y(n))^2$  [38] reaches  $NMSE \simeq 1.5 \cdot 10^{-3}$ , which is significantly better than the results reported using simulations in [17].

#### D. Experimental results

We have checked the performance of this system extensively in simulations. First of all, if we neglect the effects of the bandpass filters, and neglect all noise introduced in our experiment, we obtain a discretized system described by eq. (5) which is similar to (but nevertheless distinct from) the minimum complexity reservoirs introduced in [19]. We have checked that this discretized version of our system has performance similar to usual reservoirs on several tasks. This shows that the chosen architecture is capable of state of the art reservoir computing, and sets for our experimental system a performance goal. Secondly we have also developed a simulation code that takes into account all the noises of the experimental components, as well as the effects of the bandpass filters. These simulations are in very good agreement with the experimentally measured dynamics of the system. They allow us to efficiently explore the experimental parameter space, and to validate the experimental results. Further details on these two simulation models are given in the supplementary information.

We apply our optoelectronic reservoir to three tasks. These tasks are benchmarks which have been widely used in the reservoir computing community to evaluate the performance of reservoirs. They therefore allow comparison between our experiment and state of the art digital implementations of reservoir computing.

For the first task, we train our reservoir computer to behave like a Nonlinear Auto Regressive Moving Average equation of order 10, driven by white noise (NARMA10). More precisely, given the white noise  $u(n)$ , the reservoir should produce an output  $\hat{y}(n)$  which should be as close as possible to the response  $y(n)$  of the NARMA10 model to the same white noise. The task is described in detail in the methods section. The performance is measured by the Normalised Mean Square Error (NMSE) between output  $\hat{y}(n)$  and target  $y(n)$ . For a network of 50 nodes, both in simulations and experiment, we obtain a  $NMSE = 0.168 \pm 0.015$ . This is similar to the value obtained using digital reservoirs of the same size. For instance a NMSE value of  $0.15 \pm 0.01$  is reported in [24] also for a reservoir of size 50.

For our second task we consider a problem of practical relevance: the equalization of a nonlinear channel. We consider a model of a wireless communication channel in which the input signal  $d(n)$  travels through multiple paths to a nonlinear and noisy receiver. The task is to reconstruct the input  $d(n)$  from the output  $u(n)$  of the receiver. The model we use was



introduced in [25] and studied in the context of reservoir computing in [4]. Our results, given in Fig. 4, are one order of magnitude better than those obtained in [25] with a nonlinear adaptive filter, and comparable to those obtained in [4] with a digital reservoir. At 28 dB of signal to noise ratio, for example, we obtain an error rate of  $1.3 \cdot 10^{-4}$ , while the best error rate obtained in [25] is  $4 \cdot 10^{-3}$  and in [4] error rates between  $10^{-4}$  and  $10^{-5}$  are reported.

Finally we apply our reservoir to isolated spoken digits recognition using a benchmark task introduced in the reservoir computing community in [26]. The performance on this task is measured using the Word Error Rate (WER) which gives the percentage of words that are wrongly classified. Performances reported in the literature are a WER of 0.55% using a hidden Markov model [27]; WERs of 4.3% [26], of 0.2% [12], of 1.3% [19] for reservoir computers of different sizes and with different post processing of the output. The experimental reservoir presented in [18] reported a WER of 0.2%. Our experiment yields a WER of 0.4%, using a reservoir of 200 nodes.

Further details on these tasks are given in the methods section and in Supplementary Material 2.

### III. DISCUSSION

We have reported the first demonstration of an opto-electronic reservoir computer. Our experiment has performance comparable to state of the art digital implementations on benchmark tasks of practical relevance such as speech recognition and channel equalization. Our work demonstrates the flexibility of reservoir computers that can be readily reprogrammed for different tasks. Indeed by re-optimising the output layer (that is, choosing new readout weights  $W_k$ ), and by readjusting the operating point of the reservoir (changing the feedback gain  $\alpha$ , the input gain  $\beta$ , and possibly the bias  $\varphi$ ) one can use the same reservoir for many different tasks. Using this procedure, our experimental reservoir computer has been used successively for tasks such as signal classification, modeling a dynamical system (NARMA10 task), speech recognition, and nonlinear channel equalization.

We have introduced a new feature in the architecture, as compared to the related experiment reported in [18]. Namely by desynchronizing the input with respect to the period of the reservoir we conserve the necessary coupling between the internal states, but make a more efficient use of the internal states as the correlations introduced by the low pass filter

in [18] are not necessary.

Our experiment is also the first implementation of reservoir computing fast enough for real time information processing. It can be converted into a high speed reservoir computer simply by increasing the bandwidth of all the components (an increase of at least 2 orders of magnitude is possible with off-the-shelf optoelectronic components). We note that in future realisations it will be necessary to have an analog implementation of the pre-processing of the input (digitisation and multiplication by the input mask) and of the post-processing of the output (multiplication by output weights), rather than the digital pre- and post-processing used in the present work.

From the point of view of applications, the present work thus constitutes an important step towards building ultra high speed optical reservoir computers. To help achieve this goal, in the supplementary material we present guidelines for building experimental reservoir computers. Whether optical implementations can eventually compete with electronic implementations is an open question. From the fundamental point of view, the present work helps understanding what are the minimal requirements for high level analog information processing.

### **Acknowledgments.**

We would like to thank J. Van Campenhout whose suggestions initiated this research project. S.M. acknowledges a helpful discussion at the beginning of this project in which Ingo Fisher. All authors would like to thank the researchers of the Photonics@be network working on reservoir computing for numerous discussions over the duration of this project. The authors acknowledge financial support by Interuniversity Attraction Poles Program (Belgian Science Policy) project Photonics@be IAP6/10 and by the Fonds de la Recherche Scientifique FRS-FNRS.

### **Methods**

#### **NARMA10 task.**

Auto Regressive models and Moving Average models, and their generalisation Nonlinear Auto Regressive Moving Average Models (NARMA), are widely used to simulate time series.

The NARMA10 model is given by the recurrence

$$y(n + 1) = 0.3y(n) + 0.05y(n) \left( \sum_{i=0}^9 y(n - i) \right) + 1.5u(n - 9)u(n) + 0.1 \quad (6)$$

where  $u(n)$  is a sequence of random inputs drawn from a uniform distribution over the interval  $[0, 0.5]$ . The aim is to predict the  $y(n)$  knowing the  $u(n)$ . This task was introduced in [28]. It has been widely used as a benchmark in the reservoir computing community, see for instance [19, 24, 29]

### **Nonlinear channel equalization.**

This task was introduced in [25], and used in the reservoir computing community in [4] and [24]. The input to the channel is an i.i.d. random sequence  $d(n)$  with values from  $\{-3, -1, +1, +3\}$ . The signal first goes through a linear channel, yielding

$$\begin{aligned} q(n) = & 0.08d(n + 2) - 0.12d(n + 1) + d(n) + 0.18d(n - 1) \\ & - 0.1d(n - 2) + 0.091d(n - 3) - 0.05d(n - 4) \\ & + 0.04d(n - 5) + 0.03d(n - 6) + 0.01d(n - 7) \end{aligned} \quad (7)$$

It then goes through a noisy nonlinear channel, yielding

$$u(n) = q(n) + 0.036q(n)^2 - 0.011q(n)^3 + \nu(n) \quad (8)$$

where  $\nu(n)$  is an i.i.d. Gaussian noise with zero mean adjusted in power to yield signal-to-noise ratios ranging from 12 to 32 db. The task is, given the output  $u(n)$  of the channel, to reconstruct the input  $d(n)$ . The performance on this task is measured using the Symbol Error Rate, that is the fraction of inputs  $d(n)$  that are misclassified (Ref. [24] used another error metric on this task).

### **Isolated spoken digit recognition.**

The data for this task is taken from the NIST TI-46 corpus [30]. It consists of ten spoken digits (0...9), each one recorded ten times by five different female speakers. These 500 spoken words are sampled at 12.5 kHz. This spoken digit recording is preprocessed using the Lyon cochlear ear model [31]. The input to the reservoir  $u_j(n)$  consists of an 86-dimensional

state vector ( $j = 1, \dots, 86$ ) with up to 130 time steps. The number of variables is taken to be  $N = 200$ . The input mask is taken to be a  $N \times 86$  dimensional matrix  $b_{ij}$  with elements taken from the set  $\{-0.1, +0.1\}$  with equal probabilities. The product  $\sum_j b_{ij}u_j(n)$  of the mask with the input is used to drive the reservoir. Ten linear classifiers  $\hat{y}_k(n)$  ( $k = 0, \dots, 9$ ) are trained, each one associated to one digit. The target function for  $y_k(n)$  is  $+1$  if the spoken digit is  $k$ , and  $-1$  otherwise. The classifiers are averaged in time, and a winner-takes-all approach is applied to select the actual digit.

Using a standard cross-validation procedure, the 500 spoken words are divided in five subsets. We trained the reservoir on four of the subsets, and then tested it on the fifth one. This is repeated five times, each time using a different subset as test, and the average performance is computed. The performance is given in terms of the Word Error Rate, that is the fraction of digits that are misclassified. We obtain a WER of 0.4% (which correspond to 2 errors in 500 recognized digits).

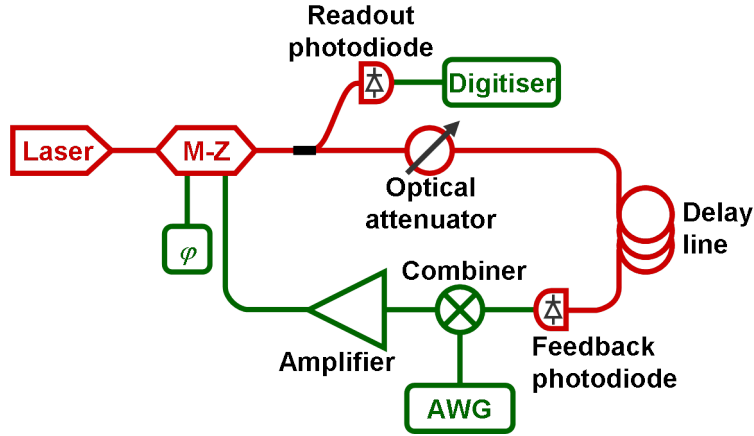


Figure 1: Scheme for the experimental set-up. The red and green parts represent respectively the optical and electronic components. The optical part of the setup is fiber based, and operates around 1550nm (standard telecommunication wavelength). “M-Z” : Lithium Niobate Mach-Zehnder modulator. “ $\varphi$ ”: DC voltage determining the operating point of the M-Z modulator. “Combiner” : electronic coupler adding the feedback and input signals. “AWG”: arbitrary waveform generator. A computer generates the input signal for a task and feeds it into the system using the arbitrary waveform generator. The response of the system is recorded by a digitiser and retrieved by the computer which optimizes the read-out function in a post processing stage. The feedback gain  $\alpha$  is adjusted by changing the average intensity inside the loop with the optical attenuator. The input gain  $\beta$  is adjusted by changing the output voltage of the function generator by a multiplicative factor. The bias  $\varphi$  is adjusted by using a DC voltage to change the operating point of the M-Z modulator. The operation of the system is fully automated and controlled by a computer using MATLAB scripts.

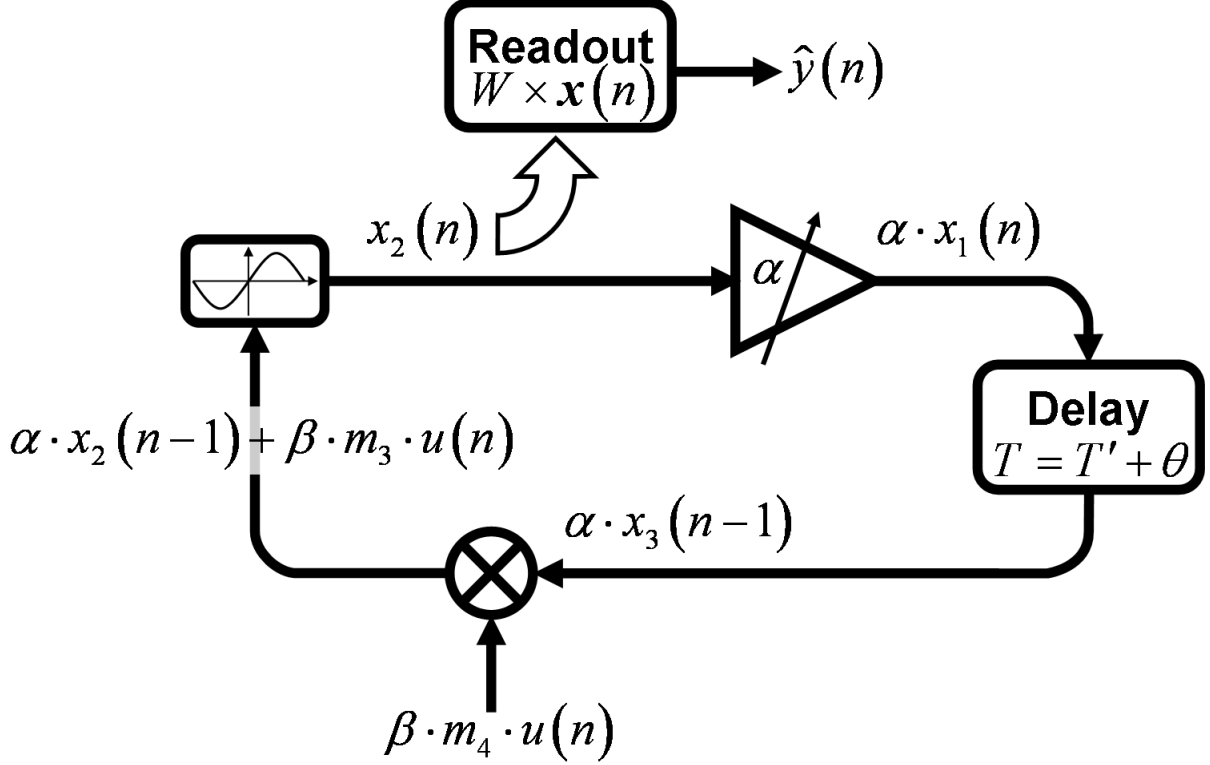


Figure 2: Schematic diagram of the information flow in the experiment depicted in Fig. 1. On the plot we have represented four reservoir nodes at different stages of processing, labelled according to equation 5 with  $k = 1$ . Starting from the bottom, and going clockwise, a input value  $u(n)$  gets multiplied by an input gain  $\beta$  and a mask value  $m_i$ , then mixed with the previous node state  $\alpha x_{i-k}(n-1)$ . The result goes through the sine function to give the new state of the reservoir  $x_i(n)$ , which then gets amplified by a factor  $\alpha$  and, after the delay, will get mixed with a new input  $u(n+1)$ . All the network states  $x_i(n)$  are also collected by the readout unit, multiplied by their respective weights  $W_i$  and added together to give the desired output  $\hat{y}(n)$ .

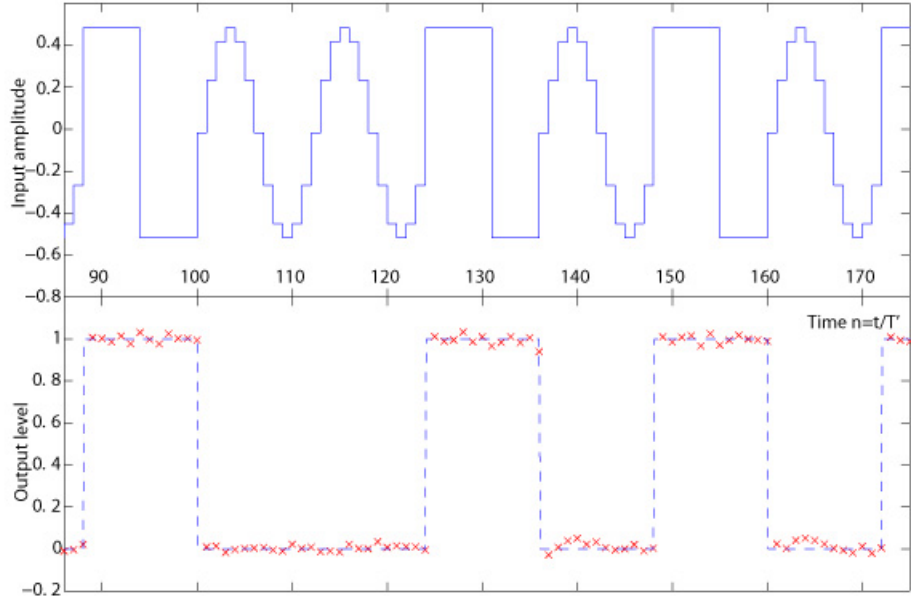


Figure 3: Signal classification task. The aim is to differentiate between square and sine waves. The top panel shows the input  $u(t)$ , a stepwise constant function resulting from the discretization of successive step and sine functions. The bottom panel shows in red crosses the output of the reservoir  $\hat{y}(n)$ . The target function (dashed line in the lower panel) is equal to 1 when the input signal is a step function and to 0 when the input signal is a sine function. The Normalized Mean Square Error, evaluated over 1000 inputs, is  $\text{NMSE} \simeq 1.5 \cdot 10^{-3}$ .

# Supplementary Material 1:

## An Introduction to Reservoir Computing for Physicists and Engineers

### Introduction

Understanding how physical systems can process information is a major scientific challenge. The tremendous progress that has been accomplished during the past century has given rise to whole new fields of science, such as computer science and digital (silicon) electronics, or quantum information. Information processing by classical analog systems is a case apart because remarkable examples are found in the biological sciences (e.g. the brain), but our understanding is still very incomplete. Thus, we understand at the basic level many aspects of how information is processed using biochemical reactions in cells, or how information is processed by neurons in a brain, to take two examples. But how these elementary processes are organized at a higher level, and what is the large scale architecture of these systems, still escapes us. Understanding these issues would be of great conceptual interest. It could also have huge technological repercussions, as it could completely change the way we build information processing machines. That this tremendous scope for progress exists is illustrated by the approximately 6 orders of magnitude gap in energy consumption between a brain and a present day silicon computer[39].

So far most work on information processing in analog systems has been based on imitating biological systems. This has given rise to the field of artificial neural networks. More abstract approaches have also been developed, such as hidden Markov models, or support vector machines. Reservoir computing [2–8] provides an alternative line of attack. The interest of reservoir computing is that 1) it proposes architectures that are quite different from those studied up to now; and 2) despite a relatively recent history -the first papers on the topic date from 2002-, its performances are comparable to, and sometimes even exceed, those of other approaches to machine learning[40]. A deeper understanding of reservoir computing could provide new insights into how analog classical systems, and in particular biological systems,



process information. Additionally it could give rise to novel approaches for implementing computation and enable new applications.

The aim of the present text is not to duplicate existing reviews of reservoir computing [9, 10]. Rather, we wish to present the subject from the point of view of the physicist or engineer who wishes to build an experimental reservoir computer. We will argue that reservoir computing provides a quite detailed, but also quite flexible, road map towards building physical systems that process information with architectures very different from those used up to now.

## Understanding Reservoir Computing

To understand the potentialities of reservoir computing, it is best to start with an example, and then examine to what extent the example can be generalized. Finally, on the basis of this discussion, we outline a road map for building experimental reservoir computers.

The archetypal reservoir computer is constructed as follows. It consists of a finite number  $N$  of internal variables  $x_i(n)$  ( $i = 0, \dots, N - 1$ ) evolving in discrete time  $n \in \mathbb{Z}$ . The evolution of the variables  $x_i(n)$  is perturbed by an external input  $u(n)$ . The evolution equations for the reservoir is:

$$x_i(n + 1) = \tanh \left[ \sum_{j=0}^{N-1} a_{ij} x_j(n) + b_i u(n) \right], \quad (9)$$

where the (time independent) coefficients  $a_{ij}$  and  $b_i$  are chosen independently at random from a simple distribution, for instance Gaussian distributions with mean zero and variances  $a^2$  and  $b^2$ . The dynamics of this system (called the “reservoir”) is fixed (i.e. the coefficients  $a_{ij}$  and  $b_i$  are fixed). The dimensionality  $N$  of the reservoir is typically much larger than the input dimensionality. Given proper parameters  $a^2$  and  $b^2$ , the reservoir will also have memory of past inputs. The use of the tanh nonlinearity in eq. (9) is traditional, but by no means essential, see below.

The aim of reservoir computing is to perform a computation on the input  $u(n)$ . To this end one maps the internal state of the reservoir to an output signal denoted  $\hat{y}(n)$ . The output should be as close as possible to a given target function  $y(n)$ . An example of this would be the detection of a stereotypical pattern in the input sequence such as spoken digits in a stream of audio, or a certain header in digital communication. Another example would

be trying to predict future inputs such as electrical load prediction or financial time-series prediction.

The output  $\hat{y}(n)$  of the reservoir computer at time  $n$  is a linear combination of the high dimensional internal states of the reservoir at time  $n$ :

$$\hat{y}(n) = \sum_{i=0}^{N-1} W_i x_i(n). \quad (10)$$

The  $W_i$  are usually chosen as follows. For some time interval,  $n \in [1, T]$  we simulate the reservoir such that one knows both the inputs  $u(n)$  and the target function  $y(n)$ . We minimize, over this training interval, the Mean Square Error between  $\hat{y}(n)$  and  $y(n)$ :

$$\text{MSE} = \frac{1}{T} \sum_{n=1}^T (\hat{y}(n) - y(n))^2. \quad (11)$$

This can be efficiently performed using standard linear regression techniques. [In cases where a classification of the inputs is desired, one may train several outputs (one for each class) and then use a winner takes all approach, or one may try to optimize the miss-classification rate using techniques such as logistic regression, Gaussian discriminant analysis, regression to the indicator function or a linear support vector machine.] Note that in general one should apply some form of regularization (to reduce the model complexity) to the readout function eq. (10). To this end one uses optimisation techniques that prefer models with small parameters  $W_i$ . This is accomplished by using e.g. ridge regression.

The coefficients  $W_i$  are now fixed and the reservoir computer is ready for use: one can input into the reservoir new inputs  $u(n)$  and obtain the corresponding output  $\hat{y}(n)$ . Because of the training procedure where we ensured proper generalization, the output will continue to be close to the target function, even for new data. It is considered good practice to check this. To this end one estimates the performance of the reservoir in a test phase during which new inputs are fed into the reservoir, and one compares, using the previously chosen  $W_i$  and an appropriate error metric, how close the output is to the target function.

Several remarks are now in order:

1. For good performance, it is necessary to scale the coefficients by a multiplicative factor

$$a_{ij} \rightarrow \alpha a_{ij} \quad \text{and} \quad b_i \rightarrow \beta b_i.$$

(In other words, if the coefficients are drawn from normal distributions with mean zero, one adjusts the variances of the normals). These parameters are often called

the feedback gain and input gain respectively. The necessity for this scaling can be understood intuitively as follows: if the coefficients  $a_{ij}$  are too small, then the state equation (9) is strongly damped; if the coefficients  $a_{ij}$  are too large, then the system has highly complex dynamics or is even chaotic, and its behavior is very sensitive to small changes in the input. The coefficients  $b_i$  are adjusted in order to have an appropriate ratio between the contribution of the terms  $\sum_j a_{ij}x_j(n)$  and the source term  $b_i u(n)$ . They also determine how non-linearly the inputs are expanded in the reservoir states.

2. Finding the optimal values of  $W_i$  is immediate in the case of linear regression. Indeed inserting eq. (10) into eq. (11) and extremizing with respect to  $W_i$ , one finds that the optimal choice is

$$W_i = \sum_{j=0}^{N-1} R_{ij}^{-1} P_j \quad (12)$$

where  $R_{ij}^{-1}$  is the inverse of the correlation matrix  $R_{ij} = \frac{1}{T} \sum_{n=1}^T x_i(n)x_j(n)$  and  $P_j = \frac{1}{T} \sum_{n=1}^T x_j(n)y(n)$ . This should be contrasted to what would happen if one tried to optimize the coefficients  $a_{ij}$  and  $b_i$ . In this case there are many more coefficients to optimize, and furthermore it is difficult to find the optimal value, as one may very easily end up in local optima. The use of a linear readout eq. (10) is thus highly advantageous.

3. Many variants on the above architecture have been investigated with success. We can list:
  - (a) Using other nonlinearities than tanh, such as the biological inspired models which approximate the way real neurons interact with each other (spiking neuron models).
  - (b) Using sparse connection matrices  $a_{ij}$  (i.e. matrices with most of the elements set to zero), so as to decrease the computational resources required to simulate the evolution.
  - (c) Using multiple inputs  $u_k(n)$ ,  $k = 1, \dots, K$ . In this case one simply adds an index to the coefficients  $b_i$ . The source term in eq. (9) thus becomes  $\sum_k b_{ik} u_k(n)$ .

- (d) Using the output  $\hat{y}(n)$  as input to the reservoir. This modification allows training the reservoir to behave as a given dynamical system [2, 4].
4. The above approach is extremely powerful. To take two examples:
- (a) Given a time series  $u(n)$  for times  $n = 1, \dots, T$ , the task is to guess the subsequent values of the time series  $u(T + 1), u(T + 2), \dots$ . The time series could for instance come from the evolution of a chaotic dynamical system, such as the Mackey-Glass system. Using the trick 3d, results which outperform all other known approaches for predicting chaotic time series were obtained [4]. Reservoir computing also won an international competition on prediction of future evolution of financial time series [11].
  - (b) Reservoir computing has been extensively applied to speech recognition. Using well known data sets, reservoir computing outperforms other approaches for isolated digit recognition [12, 14]. Recently reservoir computing has been applied to a more complex task: phoneme recognition. Performances comparable to the best alternative methods were obtained using 3 coupled reservoirs, each with  $N = 20000$  variables [13].

### **Road map for building information processing systems**

The basic setup of reservoir computing, although typically implemented in software, suggests many promising new avenues to implement computation in analog dynamic systems. The theoretical requirements for reservoir computing to be computationally universal (in the analog sense) [6] are very loose: the reservoir is required to have fading memory, to be excitable by the input and a high dimensional readout must be possible. Many physical systems could be conceived that adhere to these rules and could thus potentially be turned in universal computing machines. However turning these general ideas into a working machine is more difficult.

If one wishes to build an experimental reservoir computer, then it is essential to understand what are the constraints, but also the design freedom. In this respect, a number of important lessons can be learned from the example presented in the previous section.

1. The fact that the interconnection matrix  $a_{ij}$  and the coefficients  $b_i$  in eq. (9) are chosen at random is extremely important. It means that fine tuning of a large number of coefficients is not necessary for a good reservoir computer. Rather almost all interconnection matrices will give good performance.
2. The fact that the tanh in eq. (9) can be changed into other non-linearities is also extremely important. It means that one does not have to imitate specific non-linear behavior (such as the specific dynamics of neurons in a biological brain), but one can use the non-linearities that are easily accessible experimentally.
3. The fact that the only coefficients that are task specific are the  $W_i$  (the weights of the readout function) implies that a given dynamical system can be used for many different information processing tasks. It also implies that one can separate the design and analysis of the reservoir itself from the design and analysis of the readout function.

On the basis of these remarks, a reservoir computer can be built out of a dynamical system that satisfies the following constraints:

1. It should consist of a large number (say 50, or more, but this depends on the task and on the specifics of the dynamic system) dynamical variables which are coupled together by a non-linear evolution equation.
2. The evolution of the dynamical system can be perturbed by the external input.
3. As much as possible, one should try to break all symmetries of the system (this is the message coming from the fact that the  $a_{ij}$  and  $b_i$  are random: there is no residual structure/symmetry in the dynamics). To this end one should privilege dynamical systems that depend on a large number of random parameters.
4. A few global parameters must be experimentally tunable. These global parameters are used to adjust the operating point of the system (typically to just below the threshold of instability), and to adjust the overall weight given to the external inputs (this corresponds to the scaling of the coefficients  $a_{ij}$  and  $b_i$ ).
5. It should be possible to read-out the state of a large number (better all) of the dynamical variables, or at least to construct the readout function  $y = \sum_i W_i x_i$  with

adjustable weights  $W_i$ . Note that a reservoir computer can function satisfactorily even if only a subset of the dynamical variables are read out.

Once these constraints are satisfied, one can proceed to test the system (either using numerical simulations, or using the experimental realization). In the reservoir computing literature, there exists a series of (somewhat) standardized tests on which to evaluate the performance of the system. Some of these tests have a theoretical justification (e.g. linear memory capacity); others are interesting tasks which have been often used by the community. These tasks thus provide benchmarks with which to compare the performances of different reservoir computers. Possible tasks to study include:

1. Linear memory capacity and memory function [3]. In this task the target function  $y(n) = u(n - k)$  is simply the input  $k$  time steps in the past. Performance on this task indicates how well the reservoir's state can be used to recover past inputs. If the linear memory capacity is small, then the reservoir will be unable to carry out tasks that require long memory of the input.
2. Non-linear memory capacity, see [33, 34]. In this task the target function is a non-linear function of the past inputs, for instance the product  $y(n) = u(n - k)u(n - k')$ . Performance on this task measures how much non-linear processing of the input is carried out by the reservoir.
3. Simulating specific Nonlinear Auto Regressive Moving Average (NARMA) systems. For the NARMA tasks, the aim is to use the reservoir to simulate the response of a NARMA system driven by a random input. Two variants are widely used: a 10th order system (NARMA10) introduced in [28], and the more difficult 30th order system (NARMA30) (see for instance [35] for a definition).
4. Predicting the evolution of the trajectory of chaotic attractors such as the attractor of the Mackey-Glass system [4].
5. Speech recognition: Several benchmarks have been published, going from Japanese vowel recognition [14], to isolated spoken digits [12], to phoneme recognition [13].

This (non-exhaustive) list of benchmarks provides a natural road-map for future experimental reservoirs. First master easy tasks such as signal classification, or isolated digit

recognition. Then go on to moderately harder tasks such as NARMA10 or NARMA30. Finally, one can imagine tackling hard tasks such as phoneme recognition. In all cases, measure the linear and nonlinear memory functions, as they will give task independent information on how the reservoir is processing information.

This road-map is appealing. Steps along it have been followed using reservoirs based on water waves in a bucket [15], on the cerebral cortex of a cat [36], on analog VLSI chips [16], using a (numerically simulated) array of coupled semi-conductor optical amplifiers [17]. However it is only very recently that it has been possible, using an electronics implementation and a delayed feedback loop, to demonstrate an analog reservoir computer with performance comparable to that of digital reservoirs on a non trivial task (in this case isolated digit recognition) [18].

### **Open questions and perspectives**

The above road map leaves open a number of important questions. We outline the most obvious:

1. Effect of noise. In experimental realizations of reservoir computing, there will inevitably be noise and imperfections. How will these affect the performance of the scheme? There has not been an exhaustive analysis of this issue, but a few remarks are in order. One should distinguish between noise within the reservoir itself and noise in the readout.
  - (a) Noise in the reservoir itself is deleterious. However, reservoir computers can continue to work even with moderate levels of noise. Indeed the noise can be viewed as an unwanted input, and the aim is to perform the desired task while ignoring this second unwanted input. A possible approach to counteract the effect of noise would simply be to increase the size of the reservoir. But this remains to be studied in detail.
  - (b) Noise in the readout can be beneficial. Indeed adding noise to the readout is a trick, equivalent to ridge regularization, often used in numerical simulations to increase the robustness of reservoirs.

2. Best non-linearity. Experience with digital simulations of reservoirs shows that sigmoidal non-linearities, such as  $\tanh$ , give very good performance. However in experimental realizations, other non-linearities may be much easier to implement. Experience suggests that the best non-linearity depends to some extent on the task at hand. Also sub-optimal non-linearities can presumably be compensated by increasing the size of the reservoir.
3. Continuous time and continuous space. In numerical simulations, it is by far easier to work with a discrete set of variables  $x_i(n)$ ,  $i = 0, \dots, N - 1$  evolving in discrete time  $n \in \mathbb{Z}$ . But in experimental systems, it is often much more natural to work with continuous variables and continuous time. A theory of reservoir computing operating with continuous variables evolving in continuous time remains to be written, although some theoretical progress has been made along these lines [37].

Finally, what is the future of experimental reservoir computing? On the one hand the quest is fundamental: can we build analog systems that perform high-level information processing? Will we in this way gain new insights into how biological information processing systems operate? On the other hand experimental reservoir computers could ultimately have practical applications. Indeed they are based on architectures completely different from those used in present day digital electronics. Presumably the place to look for applications is at the frontier where digital electronics has difficulty coping, such as information processing at ultra high speeds, or with ultra low energy consumption, or for tasks which are hard to code using standard programming methods.



# Supplementary Material 2

## Experimental System, Numerical Simulations, Tasks

Here we describe in more detail our experimental system (schematized in Fig. 1 of the main text), the algorithm used to simulate it numerically, and the tasks we study to validate its performance as a reservoir.

### Undriven system

We first consider the free running dynamics of our system, in the absence of input.

The light source consists of a Laser at the wavelength 1564nm (in the standard C band of optical telecommunication). It produces a time independent intensity  $I_0$ .

The light passes through an intensity modulator (Mach-Zehnder modulator) driven by a time dependent voltage  $V(t)$ . The light intensity just after the modulator is  $I(t) = I_0 \cos^2\left(\pi\frac{V(t)}{2V_\pi} + \phi\right)$  where  $V_\pi$  is a constant voltage (the voltage which is needed to go from a maximum to the next minimum of light at the output of the modulator) and  $\phi$  can be adjusted by applying a DC bias voltage to the modulator. Taking  $\phi = 3\pi/4 + \varphi$  allows us to rewrite

$$I(t) = \frac{I_0}{2} + \frac{I_0}{2} \sin\left(\frac{\pi V(t)}{V_\pi} + \varphi\right). \quad (13)$$

The light passes through a tunable optical attenuator, enabling the adjustment of the loop's gain through the variation of the value  $I_0$ . It propagates through a long spool of fiber (1.7 km of single mode optical fiber in our experiment), and is then detected by a photodiode integrated with a transimpedance amplifier. The resulting voltage is amplified again (by a RF amplifier) to produce the voltage  $V(t)$  that drives the intensity modulator. In our experiment, the photodiode (with its transimpedance amplifier) and RF amplifier operate in a linear regime, hence  $V(t)$  is proportional to  $I(t - T)$  where  $T$  is the round trip time of the oscillator. However, one must take into account that the photodiode acts as a

lowpass filter and that the RF amplifiers act as highpass filters. Both the photodiode and the amplifiers also add noise. Thus, approximating the filters by first order filters, we have  $\tilde{V}(\omega) = A \frac{\omega_0}{\omega_0 + j\omega} \frac{j\omega}{\omega_1 + j\omega} e^{j\omega T} \left( \tilde{I}(\omega) + \tilde{n}(\omega) \right)$  where  $j$  is the imaginary unit, tilde denotes the Fourier transform,  $A$  denotes the amplification factor,  $\omega_1 \ll \omega_0$  are the cutoff frequencies of the resulting bandpass filter, and  $n(t)$  is the white noise. In the time domain we have  $V(t) = A \mathcal{F}_{\omega_0\omega_1} (I(t - T) + n(t))$  where  $\mathcal{F}_{\omega_0\omega_1}$  denotes the linear bandpass filter.

Because of the high pass filter, we can use as variable the fluctuations around the mean intensity. We define  $x(t) = \frac{I(t) - I_0/2}{I_0/2}$  (i.e., we rescale the intensity  $I(t)$  to lie in the interval  $[-1, +1]$ ) whereupon eq. (13) becomes

$$x(t) = \sin \left( \alpha \mathcal{F}_{\omega_0\omega_1} \left( x(t - T) + \frac{n(t)}{I_0} \right) + \varphi \right) \quad (14)$$

where  $\alpha = \frac{\pi A I_0}{V_\pi}$  is experimentally adjustable by changing the input light intensity  $I_0$ . Experimentally it can be tuned over the range  $\alpha \in [0, 4.2]$ .

Typical values of the parameters are  $T = 8.5\mu\text{s}$ ,  $\omega_0/2\pi = 125\text{MHz}$ ,  $\omega_1/2\pi = 50\text{kHz}$ , and the amplitude of  $n(t)/I_0$  is approximately 3.5%. At the output of the intensity modulator, an optical splitter enables us to take approximately 3% of the optical signal in order to measure the optical intensity in the fiber by the mean of a second amplified photodiode. The resulting voltage is digitized with a National Instrument PXI card at the sample rate of 200 megasamples per second, or can be measured with a digital oscilloscope.

If we increase  $I_0$  gradually, the intensity  $I(t)$  undergoes a bifurcation diagram typical of nonlinear dynamical systems. Figure 5 shows the excellent agreement between the experimentally observed bifurcation diagram and the one obtained by numerical simulations of the evolution equations (with the bias  $\varphi = 0$ ). In this bifurcation diagram, the number of bifurcations before reaching chaotic behavior is strongly affected by the amount of noise in the system. Comparing this bifurcation diagram to simulations is the most precise way we have to estimate the amount of noise in our experimental setup. The estimated value is in agreement with measurements carried out on each component of the setup separately. We also verified that the thickness of the branches inside the bifurcation diagram is mainly due to the noise level of oscilloscope.

## Driven system

We now consider the addition of an input term. The input is characterized by a new time scale  $T' \leq T$ . The scalar input  $u(n)$  (evolving in discrete time  $n \in \mathbb{Z}$ ) and the input mask  $b_i$  are transformed into a continuous input  $s(t)$  as follows:

$$s(t) = b_i u(n) \quad \text{for } t \in \left[ nT' + \frac{iT'}{N}, nT' + \frac{(i+1)T'}{N} \right], \quad i = 0, \dots, N-1, \quad n \in \mathbb{Z} \quad (15)$$

where  $N$  is the number of nodes in the reservoir. The input mask values  $b_i$ ,  $i = 0, \dots, N-1$  are randomly chosen from a given distribution (which may depend on the task). The time scale  $\theta$  over which the input  $s(t)$  changes is:

$$\theta = \frac{T'}{N}. \quad (16)$$

A voltage proportional to  $s(t)$  is generated by a function generator (at a sample rate of 200 Msamples/s) and added to the output voltage of the amplified photodiode using a RF combiner placed at the entrance of the RF amplifier. So the voltage  $V(t)$  that drives the intensity modulator is a combination of the light intensity and the input signal. The dynamical equations thus become

$$x(t) = \sin \left( \alpha \mathcal{F}_{\omega_0 \omega_1} \left( x(t-T) + \frac{n(t)}{I_0} \right) + \beta \mathcal{F}_{\omega_1} (s(t)) + \varphi \right) \quad (17)$$

where  $\beta$  is experimentally adjustable by varying the output voltage amplitude of the function generator. In this equation, we take into account that the RF combiner is placed before the RF amplifier, and therefore that the source term is affected by the highpass filter  $\mathcal{F}_{\omega_1}$  of the RF amplifier. Because of the difference between the time scales  $T$  and  $\omega_1/2\pi$ , the effect of the filter  $\mathcal{F}_{\omega_1}$  is almost negligible. Its main effect is to ensure that the effective source signal  $\mathcal{F}_{\omega_1} (s(t))$  has mean value zero.

In our experiments we take  $T = 8.5\mu s$ . The number  $N$  of variables is taken in the range 50 – 200. We take  $T' = \frac{N}{N+1}T$  (see figure 6). Thus for  $N = 50$ , we have  $\theta = 167ns$ . The performance of the reservoir does not depend on the exact value of  $T'$  chosen, as long as  $T'/T$  is not a simple fraction (such as 1, 3/4, or 1/2), which would divide our reservoir into different independent subsystems.

## Discretized dynamics

To obtain the discretized dynamics, we discretise the intensity along the fiber according to

$$x_i(n) \simeq x \left( nT' + \left( i + \frac{1}{2} \right) \theta \right) \quad i = 0, \dots, N - 1 = T'/\theta \quad (18)$$

where we suppose that  $\theta = T'/N = T/(N + k)$  with  $k$  integer (see figure 6). We thus have that the physical time  $t$  is related to  $n, i, k$  through

$$t = nT' + \left( i + \frac{1}{2} \right) \theta = \frac{(nN + (i + \frac{1}{2})) T}{N + k}. \quad (19)$$

Upon neglecting the effects of the filters  $\mathcal{F}_{\omega_0}$  and  $\mathcal{F}_{\omega_1}$  we obtain the discretized version of eq. (17). Note that the absence of synchronisation ( $T' \neq T$ , or equivalently  $k > 0$ ) completely modifies the dynamics by coupling the discretised variables  $x_i$  to each other. Note also that the wrap around effect (the second line in eq. (5)) does not appear in traditional reservoir computing.

## Numerical simulations

Two different numerical models were developed to study the capabilities of the network: a 'discretized' model, closer to the standard formulation of Echo State Networks, and a 'continuous' model, which is as close as possible to our experimental apparatus.

In the 'discretized' version of the model we implement the discretization described by eq. (5). No noise is considered, and the bandpass effects of the various components are neglected. The sine nonlinearity and the topology of the network are preserved. The optimal operating point of the system is found by tuning the parameters  $\alpha$  and  $\beta$  in eq. (5). This model is used to set a performance goal for our experimental system: if the performance of the experiment is close to the one of the model, then our system is robust enough with respect to the noise and the effects introduced by each of its components. Moreover, the performance of the 'discretized' model is the same, within the experimental error, to the one of traditional networks as reported in [24], allowing us to validate the chosen nonlinearity and topology as good choices for a reservoir computer.

The 'continuous' Matlab model we developed is instead as close as possible to the experiment. All the signals in the simulation are discretized at 200 Msamples/s. This corresponds

to the sample rate of the arbitrary waveform generator and the digitizer. All the components are represented by their transfer function at their respective operating point (sine function for the Mach-Zehnder modulator, responsivity and transimpedance gains of the photodiodes, gain of the amplifier). The collective frequency response of all the components is represented by a bandpass filter with first order slopes. This is a reasonable approximation to the exact slope of the bandpass filters which was measured using a vector network analyzer in open loop configuration. Noise is added to the signal at each noisy element of the system (dark current of the photodiode, noise added by each amplifier...).

The dynamics of the model correspond very closely to the experiment. This is illustrated for instance by the clear agreement of the simulated and measured bifurcation diagram (see fig. 5) and by the clear agreement of the simulated and measured performances on the channel equalization task, see Fig. 4 in the main text.

The continuous model allows us to easily explore the sensitivity to parameters, such as noise level or the shape of the nonlinearity, which can't always be reached with the experiment.

### **Post processing**

The light intensity  $I(t)$  in the fiber loop is converted to a voltage by a photodiode and recorded by the digitizer operating at 200MS/s. From the intensity  $I(t)$  recorded during a time  $T'$  we extract  $N$  discrete variable values  $x_i(n)$ ,  $i = 0, \dots, N - 1$ . This is carried out as follows. The intensity  $I(t)$  is divided into  $N$  pieces of duration  $\theta$ . We neglect the first quarter and the last quarter of the data points recorded over the duration  $\theta$  and associate to  $x_i(n)$  the average of the remaining data points. This procedure in which the beginning and end of each interval  $\theta$  is omitted allows us to not be affected by the transients as the intensity goes from one value to the other, and also allows an efficient synchronization of our system. The estimator  $\hat{y}(n)$  is then obtained by taking a linear combination  $\hat{y}(n) = \sum_i W_i x_i(n)$  where the weights  $W_i$  are optimized. This post processing is carried out offline, on a computer. Fig. 6 shows an example of the input sent to the reservoir, the reservoir response and the discretization operated on the reservoir output.

## Tasks

In our work we considered several tasks. We review them in detail.

### Signal classification

This is a simple task that we use for a first evaluation of the performance of the reservoir. The input  $u(n)$  to the system consists of random sequences of sine and square waves discretized into 12 points per period. The mask values  $b_i$  are drawn from the uniform distribution over the interval  $[0, +1]$ . The reservoir size is taken to be  $N = 50$ . The output  $\hat{y}(n)$  should be 1 when the signal is the square wave, and 0 when it is the sine. The weights  $W_i$  are obtained by minimizing the MSE between  $\hat{y}(n)$  and the ideal output. Experimentally we obtain  $\text{NMSE} \simeq 1.5 \cdot 10^{-3}$ , which corresponds to essentially perfect operation for this task. These experimental results are in close agreement with those obtained using numerical simulations of our reservoir.

For comparison, practically the same task was studied previously in [17]. An error rate (percentage of time the signal was misclassified) of 2.5% was obtained.

### Nonlinear channel equalization

The task is to reconstruct the input  $d(n) \in \{-3, -1, +1, +3\}$  of a noisy nonlinear wireless communication channel, given the output  $u(n)$  of the channel. The relation between  $d(n)$  and  $u(n)$  is

$$\begin{aligned} q(n) = & 0.08d(n+2) - 0.12d(n+1) + d(n) + 0.18d(n-1) \\ & - 0.1d(n-2) + 0.091d(n-3) - 0.05d(n-4) \\ & + 0.04d(n-5) + 0.03d(n-6) + 0.01d(n-7) \end{aligned} \tag{20}$$

$$u(n) = q(n) + 0.036q(n)^2 - 0.011q(n)^3 + \nu(n) \tag{21}$$

where  $\nu(n)$  represents i.i.d. Gaussian noise with zero mean, adjusted in power to yield signal-to-noise ratios ranging from 12 to 32 dB. This task was introduced in [25] and it was shown in [4] that reservoir computing could significantly improve performance on this task.

In our study, the input mask is taken to be uniformly distributed over the interval  $[-1, +1]$ . The reservoir size is taken to be  $N = 50$ . To perform the task, we first obtain an estimator  $\hat{y}(n)$  of the input by minimizing the MSE between  $\hat{y}(n)$  and  $d(n)$ . We then obtain an estimator  $\hat{d}(n)$  by replacing  $\hat{y}(n)$  by the discretized value  $\{-3, -1, +1, +3\}$  to which it is closest. Finally we estimate the Symbol Error Rate (SER), i.e., the fraction of time that  $\hat{d}(n)$  differs from  $d(n)$ . The performance of the network is calculated as the average performance over 10 different input sequences, in which the first 3000 samples form the training set and the following 6000 samples form the test set. The SER on the test set is then studied as a function of Signal to Noise Ratio at the input. The values reported in figure 4 in the main text are the average SER for 10 different trials, while the error bars represent the standard deviation of the SER for the same trials. It should be noted that 6000 test steps are the maximum number of steps that the arbitrary waveform generator in our setup allows. Hence, when SERs approach  $10^{-4}$ , our average SERs include trials where two errors, one error, or no error at all have been made by the reservoir. This means that the error bars on the experimental data where SERs are close to  $10^{-4}$  might be overestimated. In contrast, data from simulations do not suffer from this effect, as we can arbitrarily increase the number of test samples for a more precise measurement.

For comparison, at a SNR ratio of 28dB, the three models studied in [25] gave SER of  $2 \cdot 10^{-3}, 4 \cdot 10^{-3}, 1.5 \cdot 10^{-2}$ , while the reservoir studied in [4] gave SERs of  $1 \cdot 10^{-4}$  to  $1 \cdot 10^{-5}$ . At the same SNR of 28dB, our experimental system gives a SER of  $1.3 \cdot 10^{-4}$ .

## NARMA10

In this task the aim is to reproduce the behavior of a nonlinear, tenth-order system with random input drawn from a uniform distribution over the interval  $[0, 0.5]$ . The equation defining the target system is given by

$$y(n+1) = 0.3y(n) + 0.05y(n) \left( \sum_{i=0}^9 y(n-i) \right) + 1.5u(n-9)u(n) + 0.1 \quad (22)$$

For this task, the mask is uniformly distributed over  $[0, +1]$  and the reservoir size is  $N = 50$ . We first train our system using 1000 time steps, then we test the system on a new sequence of 1000 inputs. The performance of the reservoir is measured by the Normalized Mean Square Error of the estimator  $\hat{y}(n)$ , averaged over 10 different pairs of train and

test sequences. For this NARMA10 task, the best performances (NMSE = 0.16 for the discretized simulation, 0.168 for the continuous simulation and 0.167 for the experiment ) are obtained in a very linear regime.

### Isolated spoken digit recognition

For the isolated spoken digit recognition task, the data is taken from the NIST TI-46 corpus [30]. It consists of ten spoken digits (0..9), each one recorded ten times by five different female speakers. These 500 spoken words are sampled at 12.5 kHz. This spoken digit recording is preprocessed using the Lyon cochlear ear model [31]. The input to the reservoir  $u_j(n)$  consists of an 86-dimensional state vector ( $j = 1, \dots, 86$ ) with up to 130 time steps. The number of variables is taken to be  $N = 200$ . The input mask is taken to be a  $N \times 86$  dimensional matrix  $b_{ij}$  with elements taken from the the set  $\{-0.1, +0.1\}$  with equal probabilities. The product  $\sum_j b_{ij}u_j(n)$  of the mask with the input is used to drive the reservoir. Ten linear classifiers  $\hat{y}_k(n)$  ( $k = 0, \dots, 9$ ) are trained, each one associated to one digit. The target function for  $y_k(n)$  is +1 if the spoken digit is  $k$ , and -1 otherwise. The classifiers are averaged in time, and a winner-takes-all approach is applied to select the actual digit.

In our study, the 500 spoken words are divided in five subsets. We trained the reservoir on four of the subsets, and then tested it on the fifth one. This is repeated five times in order to use each subset as test part. In this way we can test our system over all the speakers and digits, and compute an average performance . The performance is given in terms of the Word Error Rate, that is the fraction of digits that are misclassified. We obtain a WER of 0.4% which correspond to 2 errors in 500 recognized digits.

For comparison, in [26], where Reservoir Computing was first used on this spoken digit benchmark, a WER of 4.3% was reported for a reservoir of size 1232. In [12] a WER of 0.2% was obtained for a reservoir of size 308 and using the winner-takes-all approach. In [19] a WER of 1.3% for reservoirs of size 200 is reported. The experimental reservoir reported in [18] gives a WER of 0.2% using a reservoir of size 400. The Sphinx-4 system [27] uses a completely different method based on Hidden Markov Models and achieves a WER of 0.55% on the same data set.



- 
- [1] H. John Caulfield and Shlomi Dolev. Why future supercomputing requires optics. *Nature Photonics*, 4(5):261–263, 2010.
- [2] H. Jaeger. The "echo state" approach to analysing and training recurrent neural networks. Technical report, Technical Report GMD Report 148, German National Research Center for Information Technology, 2001.
- [3] H. Jaeger. Short term memory in echo state networks. Technical report, Technical Report GMD Report 152, German National Research Center for Information Technology, 2001.
- [4] Herbert Jaeger and Harald Haas. Harnessing nonlinearity: predicting chaotic systems and saving energy in wireless communication. *Science (New York, N.Y.)*, 304(5667):78–80, 2004.
- [5] Robert Legenstein and Wolfgang Maass. *New Directions in Statistical Signal Processing: From Systems to Brain*, chapter What makes a dynamical system computationally powerful?, pages 127–154. MIT Press, 2005.
- [6] Wolfgang Maass, T. Natschläger, and Henry Markram. Real-time computing without stable states: A new framework for neural computation based on perturbations. *Neural computation*, 14(11):2531–2560, 2002.
- [7] J.J. Steil. Backpropagation-decorrelation: online recurrent learning with  $O(N)$  complexity. *2004 IEEE International Joint Conference on Neural Networks (IEEE Cat. No.04CH37541)*, pages 843–848.
- [8] David Verstraeten, Benjamin Schrauwen, M D’Haene, and Dirk Stroobandt. An experimental unification of reservoir computing methods. *Neural networks : the official journal of the International Neural Network Society*, 20(3):391–403, 2007.
- [9] Mantas Lukoševičius and Herbert Jaeger. Reservoir computing approaches to recurrent neural network training. *Computer Science Review*, 3(3):127–149, 2009.
- [10] Barbara Hammer and Benjamin Schrauwen. Recent advances in efficient learning of recurrent networks. In *Proceedings of the European Symposium on Artificial Neural Networks*, pages 213–216, 2009.
- [11] <http://www.neural-forecasting-competition.com/NN3/index.htm>.
- [12] David Verstraeten, Benjamin Schrauwen, and Dirk Stroobandt. Reservoir-based techniques for speech recognition. In *The 2006 IEEE International Joint Conference on Neural Network*

- Proceedings*, pages 1050–1053. IEEE, 2006.
- [13] Fabian Triefenbach, A. Jalalvand, Benjamin Schrauwen, and J. Martens. Phoneme recognition with large hierarchical reservoirs. *Advances in Neural Information Processing Systems*, 23:1–9, 2010.
- [14] Herbert Jaeger, Mantas Lukosevicius, Dan Popovici, and Udo Siewert. Optimization and applications of echo state networks with leaky-integrator neurons. *Neural networks : the official journal of the International Neural Network Society*, 20(3):335–52, 2007.
- [15] Chrisantha Fernando and Sampsa Sojakka. Pattern recognition in a bucket. In Wolfgang Banzhaf, Jens Ziegler, Thomas Christaller, Peter Dittrich, and Jan Kim, editors, *Advances in Artificial Life*, volume 2801 of *Lecture Notes in Computer Science*, pages 588–597. Springer Berlin / Heidelberg, 2003.
- [16] Felix Schüzgermann, Karlheinz Meier, and Johannes Schemmel. Edge of chaos computation in mixed-mode vlsi - a hard liquid. In *Advances in Neural Information Processing Systems*. MIT Press, 2005.
- [17] Kristof Vandoorne, Wouter Dierckx, Benjamin Schrauwen, David Verstraeten, Roel Baets, Peter Bienstman, and Jan Van Campenhout. Toward optical signal processing using photonic reservoir computing. *Optics express*, 16(15):11182–92, 2008.
- [18] L. Appeltant, M.C. Soriano, G. Van der Sande, J. Danckaert, Serge Massar, J. Dambre, Benjamin Schrauwen, C. R. Mirasso, and I. Fischer. Information processing using a single dynamical node as complex system. *submitted to Nat. Comm.*, 2011.
- [19] Ali Rodan and Peter Tino. Minimum complexity echo state network. *IEEE transactions on neural networks*, 22(1):131–44, 2011.
- [20] Thomas Erneux. *Applied Delay Differential Equations*. Springer, 2009.
- [21] Laurent Larger, Pierre-Ambroise Lacourt, Stéphane Poinsot, and Marc Hanna. From flow to map in an experimental high-dimensional electro-optic nonlinear delay oscillator. *Physical Review Letters*, 95(4):1–4, 2005.
- [22] Yanne K. Chembo, Pere Colet, Laurent Larger, and Nicolas Gastaud. Chaotic Breathers in Delayed Electro-Optical Systems. *Physical Review Letters*, 95(20):2–5, 2005.
- [23] Michael Peil, Maxime Jacquot, Yanne K. Chembo, Laurent Larger, and Thomas Erneux. Routes to chaos and multiple time scale dynamics in broadband bandpass nonlinear delay electro-optic oscillators. *Physical Review E*, 79(2):1–15, 2009.

- [24] Ali Rodan and Peter Tino. Simple Deterministically Constructed Recurrent Neural Networks. *Intelligent Data Engineering and Automated Learning - IDEAL 2010*, pages 267–274, 2010.
- [25] V. John Mathews and Junghsi Lee. Adaptive algorithms for bilinear filtering. *Proceedings of SPIE*, 2296(1):317–327, 1994.
- [26] David Verstraeten, Benjamin Schrauwen, and Dirk Stroobandt. Isolated word recognition using a liquid state machine. In *Proceedings of the 13th European Symposium on Artificial Neural Networks (ESANN)*, pages 435–440, 2005.
- [27] Willie Walker, Paul Lamere, Philip Kwok, Bhiksha Raj, Rita Singh, Evandro Gouvea, Peter Wolf, and Joe Woelfel. Sphinx-4: a flexible open source framework for speech recognition. Technical report, Mountain View, CA, USA, 2004.
- [28] Amir F. Atiya and Alexander G. Parlos. New results on recurrent network training: unifying the algorithms and accelerating convergence. *IEEE transactions on neural networks*, 11(3):697–709, 2000.
- [29] H. Jaeger. Adaptive Nonlinear System Identification with Echo State Networks. In *Advances in Neural Information Processing Systems*, volume 8, pages 593–600. MIT Press, 2002.
- [30] Texas Instruments-Developed 46-Word Speaker-Dependent Isolated Word Corpus (TI46), September 1991, NIST Speech Disc 7-1.1 (1 disc), 1991.
- [31] R. Lyon. A computational model of filtering, detection, and compression in the cochlea. In *ICASSP '82. IEEE International Conference on Acoustics, Speech, and Signal Processing*, pages 1282–1285. Institute of Electrical and Electronics Engineers, 1982.
- [32] Rajagopal Ananthanarayanan, Steven K. Esser, Horst D. Simon, and Dharmendra S. Modha. *The cat is out of the bag: : cortical simulations with  $1^{09}$  neurons,  $10^{13}$  synapses*. SC '09. ACM, New York, NY, USA, 2009.
- [33] David Verstraeten, Joni Dambre, Benjamin Schrauwen, and Serge Massar. Linear and nonlinear memory capacity of dynamical systems. *in preparation*.
- [34] David Verstraeten, Joni Dambre, Xavier Dutoit, and Benjamin Schrauwen. Memory versus non-linearity in reservoirs. In *The 2010 International Joint Conference on Neural Networks (IJCNN)*, pages 1–8. IEEE, July 2010.
- [35] Benjamin Schrauwen, M Wardermann, David Verstraeten, J.J. Steil, and Dirk Stroobandt. Improving reservoirs using intrinsic plasticity. *Neurocomputing*, 71(7-9):1159–1171, 2008.
- [36] Danko Nikolic, Stefan Hiçeusler, Wolf Singer, and Wolfgang Maass. Temporal dynamics of

- information content carried by neurons in the primary visual cortex. *Advances in Neural Information Processing Systems*, 19:1041–1048, 2007.
- [37] Michiel Hermans and Benjamin Schrauwen. Memory in linear recurrent neural networks in continuous time. *Neural networks : the official journal of the International Neural Network Society*, 23(3):341–55, 2010.
- [38] Note that, although reservoirs are usually trained using linear regression, i.e., minimizing the MSE, they are often evaluated using other error metrics. In order to be able to compare with previously reported results, we have adopted the most commonly used error metric for each task.
- [39] To simulate (with a speed reduction of 2 orders of magnitude) a cat brain that consumes roughly 1 Watt, the Blue Gene supercomputer consumes roughly a  $10^6$ Watt. For a presentation of the simulation, see [32]
- [40] Machine learning is the field of artificial intelligence concerned with developing algorithms whose response to the input -typically empirical data- improves with experience.

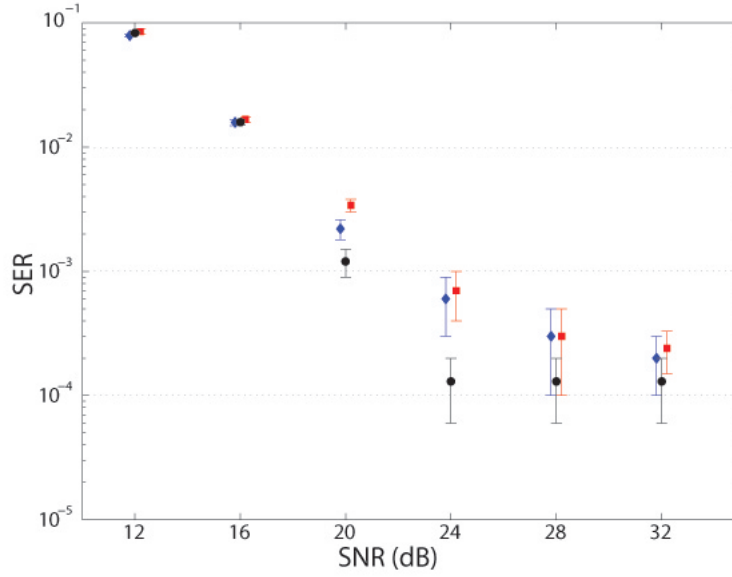


Figure 4: Results for nonlinear channel equalization. The horizontal axis is the Signal to Noise Ratio (SNR) of the channel. The vertical axis is the Symbol Error Rate (SER), that is the fraction of input symbols that are misclassified. Results are plotted for the experimental setup (black circles), the discrete simulations based on eq. (5) (blue rhombs), and the continuous simulations that take into account noise and bandpass filters in the experiment (red squares). All three sets of results agree within the statistical error bars. Error bars on the experimental points relative to 24, 28 and 32 dB might be overestimated (see Supplementary Material 2). The results are practically identical to those obtained using a digital reservoir in [4].

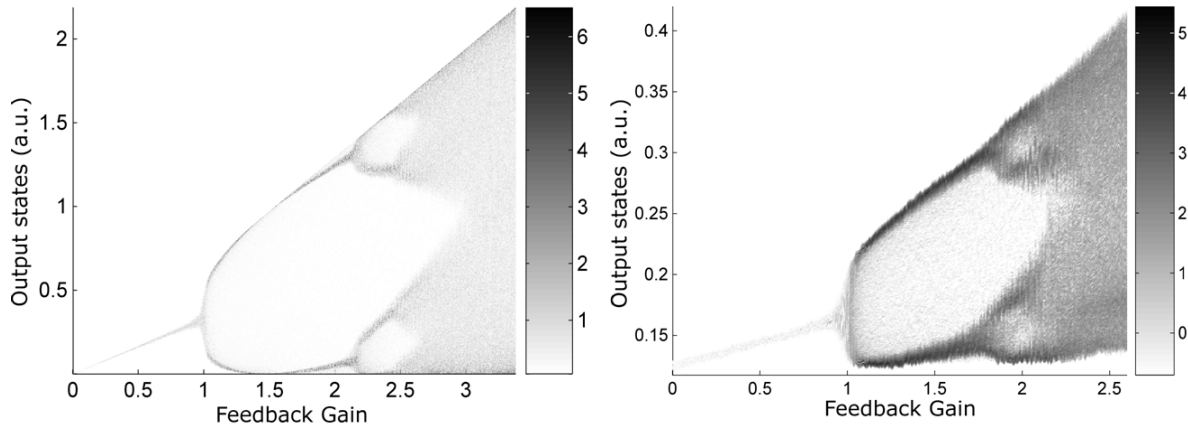


Figure 5: Simulated (left panel) and measured (right panel) bifurcation diagram. The vertical axis (output states) is proportional to the optical intensity in the optical fiber for the simulations, and to the voltage at the output of the readout photodiode for the measurements (this voltage is equal to de optical intensity multiplied by the gain of the amplified photodiode). The gray scale represents the histogram of optical intensities inside the system as a function of the feedback gain. When the feedback gain is lower than unity, only one value of the light intensity is possible. For feedback gain slightly larger than unity, the light intensity oscillates between two values. For even larger feedback gain (around 2), the nonbijective nature of the Mach-Zehnder modulator’s transfer function leads to oscillation between multiple light intensity levels or even to a chaotic behavior. The number of bifurcations before reaching the chaotic behavior is determined by the amount of noise inside the system. The thickness of the branches in the measured bifurcation diagram is due to the noise added by the oscilloscope.

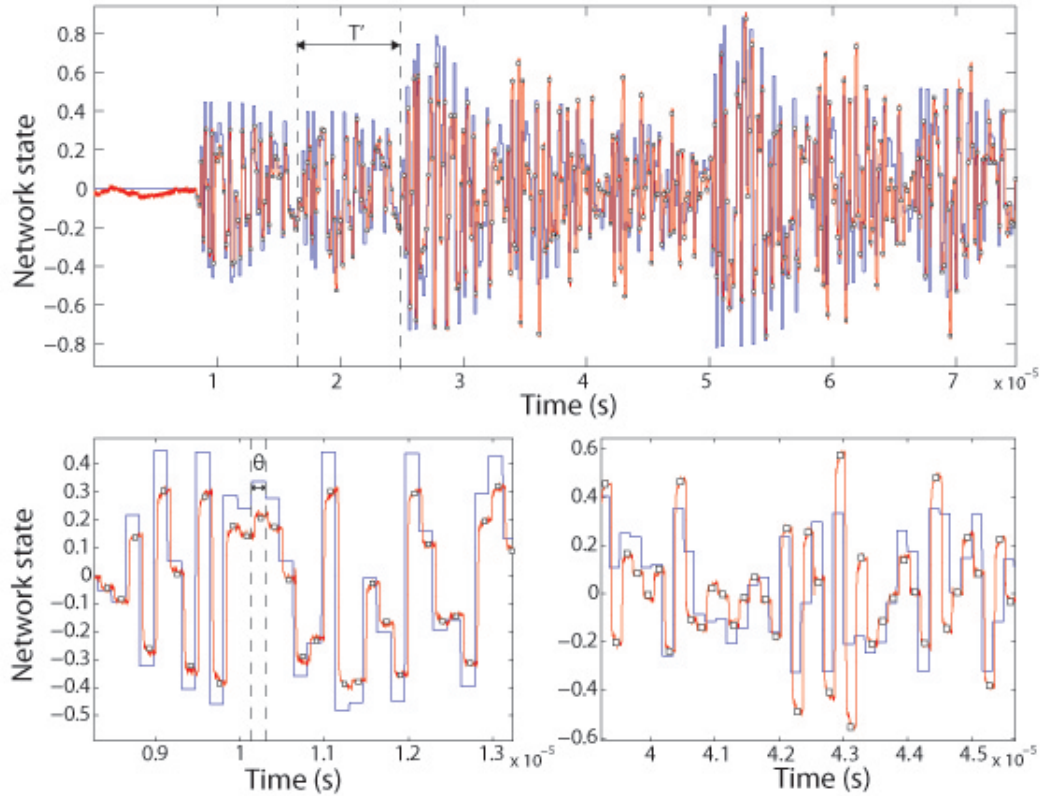


Figure 6: Operation of the experimental reservoir. The blue line represents the masked input driving the reservoir; the red line represents the reservoir response to the depicted input as measured by the oscilloscope. Both have been normalized so that their values lie between -1 and 1 for the whole length of the experiment. The white squares along the red line represent the discretized values of the reservoir states, obtained by averaging the reservoir output on a time interval of amplitude  $\theta/2$ . The upper part of the figure shows the reservoir operation for the first 8 inputs of the reservoir; note that the input is zero up to  $t \approx 0.8 \cdot 10^{-5}$ . The bottom left panel shows a detail from the measurement on the response to the very first input value, when no feedback is present yet, and we only see the instantaneous response of the Mach-Zehnder. The panel on the bottom right depicts the response of the system to the 5th input, where the effect of the feedback is clearly visible: the amplitudes of the reservoir states are no longer just related to the instantaneous input, but are influenced by previous inputs as well.